Neoplasia • Vol. 5, No. 4, July/August 2003, pp. 308–318 308

www.neoplasia.com

Tumor Oxygen Dynamics: Correlation of *In Vivo* MRI with Histological Findings[1]

Dawen Zhao, Sophia Ran†, Anca Constantinescu*, Eric W. Hahn* and Ralph P. Mason**

Departments of *Radiology and †Pharmacology, UT Southwestern Medical Center, Dallas, TX, USA

Abstract

Tumor oxygenation has long been recognized as a significant factor influencing cancer therapy. We recently established a novel magnetic resonance *in vivo* approach to measuring regional tumor oxygen tension, *FREDOM* (Fluorocarbon Relaxometry Using Echo Planar Imaging for Dynamic Oxygen Mapping), using hexafluorobenzene (HFB) as the reporter molecule. We have now investigated oxygen dynamics in the two Dunning prostate R3327 rat tumor sublines, AT1 and H. *FREDOM* revealed considerable intratumoral heterogeneity in the distribution of pO_2 values in both sublines. The anaplastic faster-growing AT1 tumors were more hypoxic compared with the size-matched, well-differentiated, and slower-growing H tumors. Respiratory challenge with oxygen produced significant increases in mean and median pO_2 in all the H tumors ($P<.001$), but no response in half of the larger AT1 tumors (>3 cm^3). Immunohistochemical studies using the hypoxia marker, pimonidazole, and the vascular endothelial cell marker, CD31, confirmed that the H tumors had more extensive vasculature and less hypoxia than the AT1 tumors. These results further validate the utilization of *FREDOM* to monitor tumor oxygenation and concur with the hypothesis that the level of hypoxia is related to tumor growth rate and poor vascularity.

Neoplasia (2003) **5,** 308–318

Keywords: ^{19}F nuclear magnetic resonance (NMR); oxygen tension; prostate tumor; immunohistochemistry; hypoxia.

Introduction

It is well recognized that hypoxia in solid tumors affects response to radiotherapy [1–3] and some chemotherapeutic drugs [4]. Recent evidence, in experimental and clinical studies, indicates that tumor hypoxia might also be a mechanism for malignant progression and metastasis in solid tumors [5,6]. Given the importance of oxygen, many techniques for monitoring pO_2 have been developed [7]. Although each method has specific attributes, many are highly invasive and impractical for longitudinal studies of specific regions of interest.

We recently demonstrated the feasibility of measuring tumor oxygenation based on ^{19}F nuclear magnetic resonance (NMR) echo planar imaging (EPI) following direct intratumoral injection of the reporter molecule, hexafluorobenzene (HFB) — *FREDOM* (Fluorocarbon Relaxometry Using Echo Planar Imaging for Dynamic Oxygen Mapping) [8]. This technique allows us to not only simultaneously examine multiple specific locations within a tumor, but also observe dynamic changes at individual locations with respect to intervention. Our previous studies of Dunning R3327 prostate rat tumor sublines have demonstrated that the faster-growing metastatic MAT-Lu tumors were more hypoxic than the relatively well-differentiated and slower-growing HI tumors [9]. In order to further investigate the potential correlation between hypoxia and tumor malignant progression, we have now studied and compared tumor oxygen tension dynamics in two other Dunning prostate rat tumor sublines: the well-differentiated and slower-growing H and the anaplastic fast-growing AT1, which derives originally from the course of passage of the H [10].

There is a close relationship between hypoxia and vascular extent in solid tumors, and it is widely accepted that tumor hypoxia results in part from poor vascularity [11]. Immunohistochemistry based on bioreductive chemical markers and vascular endothelial cell markers can reveal spatial patterns of tumor hypoxia and vasculature, as well as their relationship at the cellular level [12–14]. We have now compared direct pO_2 measurements using *FREDOM* with histological investigations of hypoxia and vasculature using pimonidazole and anti-CD31 antibody, and show that the macroscopic dynamic imaging is consistent with the histological microstructure.

Abbreviations: EPI, echo planar imaging; *FREDOM*, Fluorocarbon Relaxometry Using Echo Planar Imaging for Dynamic Oxygen Mapping; HF, hypoxic fraction; HFB, hexafluorobenzene; VDT, volume doubling time

Address all correspondence to: Ralph P. Mason, PhD, C Chem, Department of Radiology, UT Southwestern Medical Center, 5323 Harry Hines Boulevard, Dallas, TX 75390-9058, USA. E-mail: ralph.mason@utsouthwestern.edu

[1]This research was supported, in part, by NIH RO1 CA79515 (NCI)/EB002762 (NIBIB) and the DOD Prostate Cancer Initiative Postdoctoral Award (DAMD 170110108) (D.Z.), and performed in conjunction with Cancer Imaging Program P20 CA 86354.

Received 23 January 2003; Accepted 25 April 2003.

Methods

Experiments were approved by the Institutional Animal Care and Research Advisory Committee.

Tumor Model

Two sublines of the Dunning prostate R3327 adenocarcinoma were selected: H, a well-differentiated and slow-growing tumor with volume doubling time (VDT) of 16 days [15], and AT1, an anaplastic and faster-growing subline with VDT of 5 days [10]. Tumors were originally obtained from Dr. J. T. Isaacs (Johns Hopkins, Baltimore, MD) and provided to us by Dr. P. Peschke (DKFZ, Heidelberg, Germany). Tumors were implanted in a skin pedicle surgically created on the foreback of adult male Copenhagen-2331 rats (~250 g; Harlan, Indianapolis, IN), as described in detail previously [16]. Tumors were allowed to grow and were investigated by magnetic resonance imaging (MRI) when about 1 cm^3 or when >3 cm^3 (~10 mm or >20 mm in diameter). Twelve H tumors, including six small (size range 0.6–1.5 cm^3) and six large tumors (range 3.0–4.6 cm^3), and 13 AT1 tumors, including seven small (range 0.7–1.8 cm^3) and six large tumors (range 3.0–5.2 cm^3), were investigated. In preparation for MRI, each rat was given ketamine hydrochloride (200 μl, 100 mg/ml, i.p.; Aveco, Fort Dodge, IA) as a relaxant and maintained under general gaseous anesthesia (1 dm^3/min air and 1.3% isoflurane; Baxter International, Deerfield, IL). HFB (50 μl; Lancaster, Gainesville, FL) was deoxygenated by bubbling nitrogen for 5 minutes before use, and injected directly into the tumors using a Hamilton syringe (Hamilton, Reno, NV) with a custom-made fine sharp needle (32 gauge), as described in detail previously [9]. Generally, HFB was administered along three tracks in the form of a fan in a single central plane of the tumor coronal to the rat's body. The needle was inserted manually to penetrate across the whole tumor and withdrawn ~1 mm to reduce pressure, and 3 μl of HFB was deposited. The needle was repeatedly withdrawn a

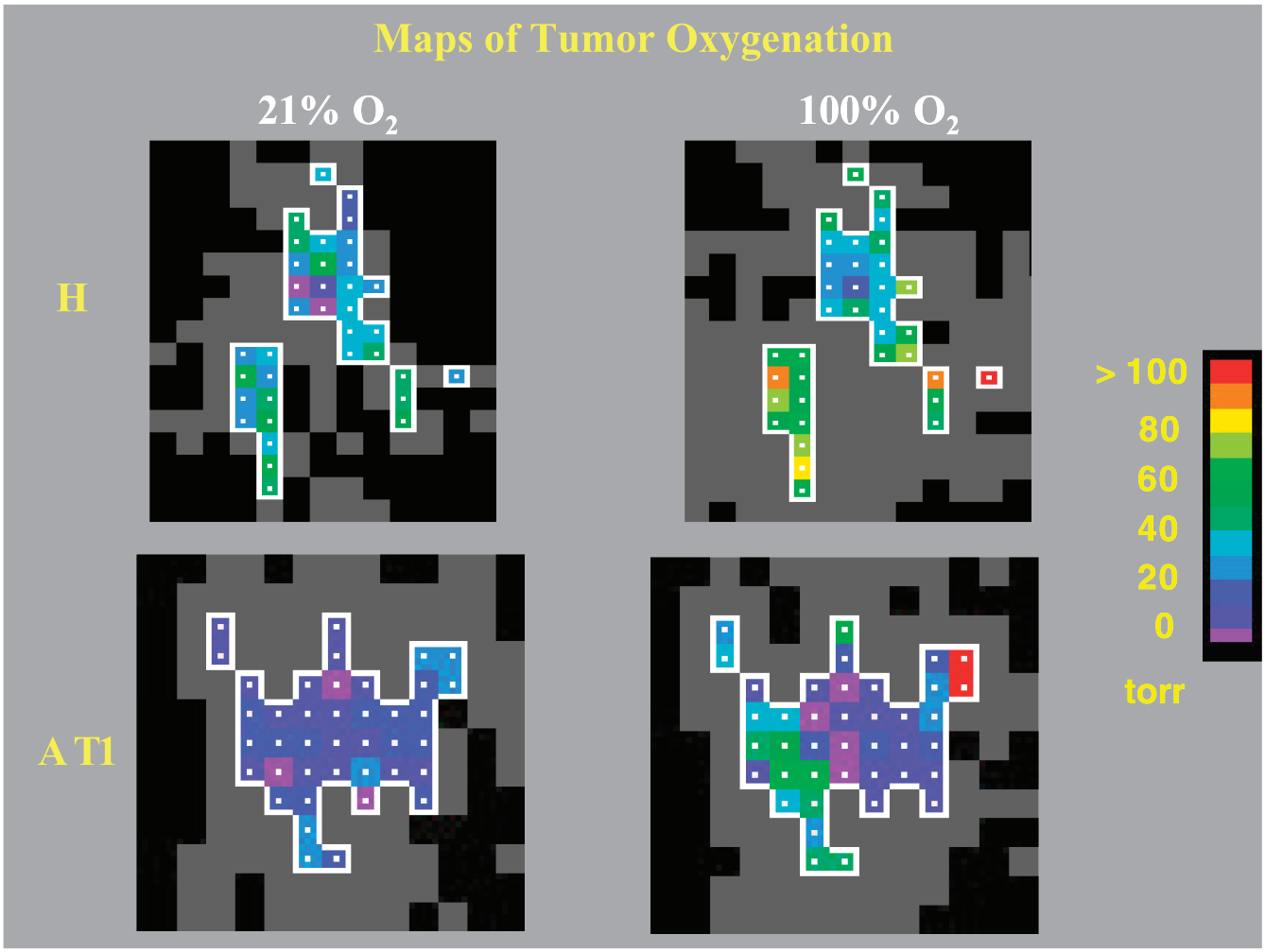

Figure 1. *pO_2 maps obtained using FREDOM. Distinct heterogeneity was seen in these representative small H (1.1 cm^3) and AT1 (1.5 cm^3) tumors under baseline conditions, when the anesthesized rats breathed air. The H tumor [baseline mean pO_2=20.3±2.2 (SE) Torr] was significantly better oxygenated than the AT1 tumor (baseline mean pO_2=5.3±0.9 Torr, P<.001). In response to oxygen inhalation, pO_2 increased significantly in both the H and the AT1 tumors [mean pO_2=46.7±3.7 Torr (P<.001) and 17.2±3.8 Torr (P<.005), respectively]. In each case, the fourth measurement after switching to oxygen breathing is shown. Colored voxels were selected by applying threshold criteria to each ensuring high-quality data throughout the time course. Gray voxels provided a T1 curve fit, but with large errors.*

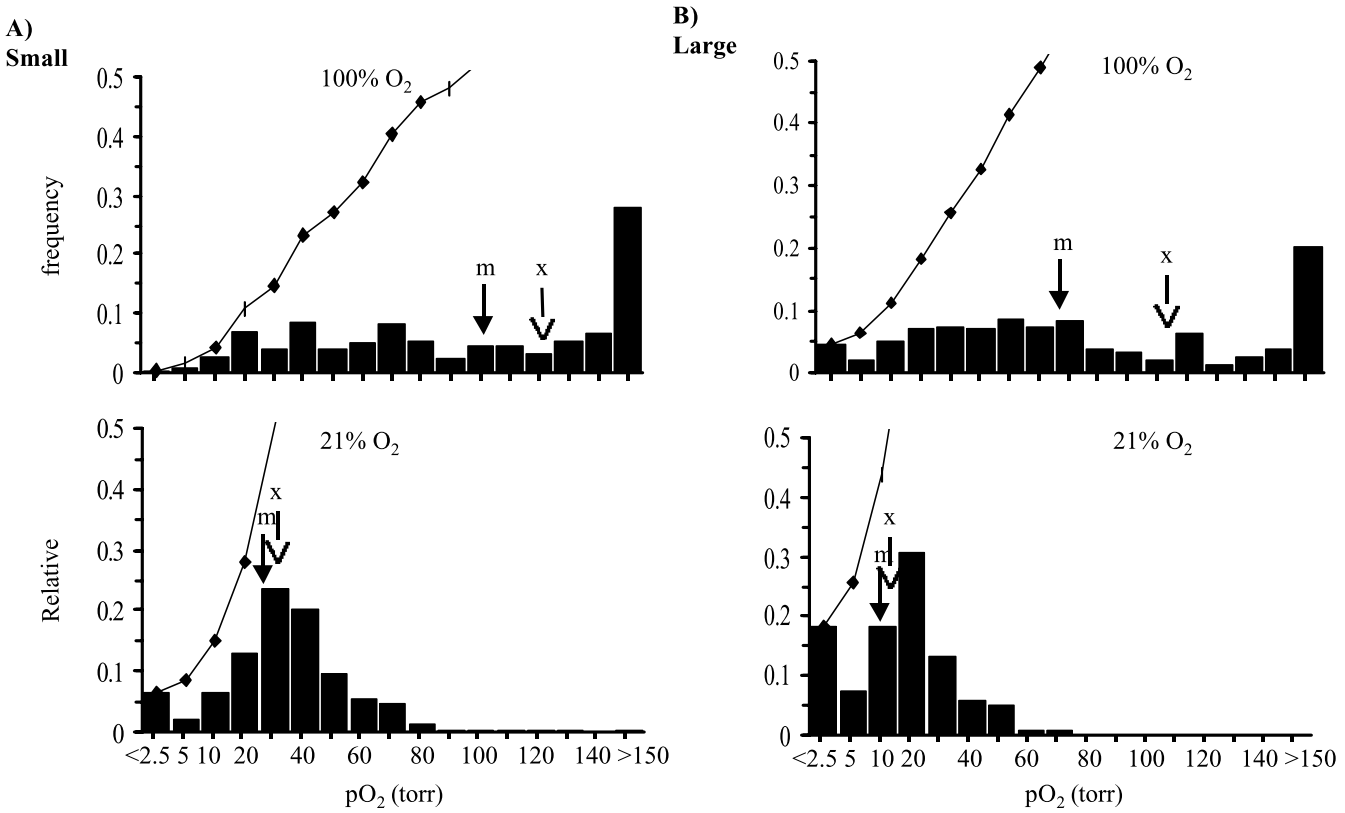

Figure 2. *Histograms of tumor oxygenation pooled for the H tumors. Data from six small (219 voxels) and six large (159 voxels) H tumors obtained using FREDOM show distinct heterogeneity. The small tumors (A) were significantly better oxygenated (mean = 31 ± 2 Torr, median = 27 Torr) than the large tumors (B) (mean = 14 ± 1 Torr, median = 12 Torr; P<.001). In response to respiratory challenge with oxygen, both mean and median pO_2 in each group increased significantly (P<.001). Arrows indicate mean (x) and median (m) pO_2, respectively. The bin numbers show the maximum pO_2 for each category. Cumulative frequencies are shown by curves.*

further 2 to 3 mm and additional HFB was deposited. Typically, HFB was deliberately deposited at about 16 individual locations per tumor, in both the central and peripheral regions of the tumors, to ensure that the interrogated regions would be representative of the whole tumor. Each animal was placed on its side in a cradle with a thermal blanket to maintain body temperature.

Tumor Oximetry — FREDOM

Magnetic resonance experiments were performed using an Omega CSI 4.7 horizontal bore magnet system with actively shielded gradients (Bruker Instrument, Fremont, CA). A tunable ($^1H/^{19}F$) MR coil, 2 or 3 cm in diameter matched to the tumor size (constructed from a cylindrical copper tube about 2 cm deep and acting as a single-turn solenoid), was placed around the tumor-bearing pedicle. Proton images were obtained for anatomical reference using a three-dimensional (3D) spin-echo sequence. The coil was then retuned in place to 188.27 MHz, and corresponding [^{19}F]MR images were obtained. Overlaying the [^{19}F]MR images on the corresponding proton images revealed the distribution of HFB.

Following conventional MR imaging, tumor oxygenation was estimated on the basis of ^{19}F pulse burst saturation recovery (PBSR) EPI relaxometry of the HFB, as described previously [8]. The *ARDVARC* (Alternated R1 Delays with Variable Acquisitions to Reduce Clearance effects) data acquisition protocol was applied to optimize data quality. This approach provided pO_2 maps with 1.25 mm in-plane voxel resolution in 8 minutes with typically ~50 to 150 individual pO_2 measurements (voxels per tumor). The spin–lattice relaxation rate [R1 (sec^{-1})=1/T1] was estimated on a voxel-by-voxel basis using a three-parameter monoexponential function, and pO_2 was estimated using the relationship pO_2 (Torr)=(R1−0.0835)/0.001876 [8]. Three consecutive baseline pO_2 measurements were made over 24 minutes while the rats breathed air. The inhaled gas was then altered to oxygen (100% O_2) and pO_2 maps were immediately acquired with no equilibration period. Five consecutive maps were acquired over 40 minutes. The gas was then returned to air, and five further maps were acquired over 40 minutes.

Histology

Histological studies were performed on large AT1 and H tumors.

Necrosis

For H&E staining, tumor tissues were fixed in 10% formalin, embedded in paraffin, and sectioned (4 μm). Tumor necrotic regions were identified on the H&E stained slides examined under low magnification (×2 objective). All fields (~30) in each section were captured by a digital camera and

processed using Metaview software (Universal Imaging, West Chester, PA). Fields were calibrated according to magnification, and areas occupied by necrotic cells were outlined, calculated, and expressed in square millimeters. The area of the entire cross section was determined manually. The proportion of necrotic areas (% necrosis) was calculated as follows: sum of all necrotic areas in a single cross section divided by total area of cross section and multiplied by 100. Five slides representing each tumor type were analyzed and the percentage of necrosis was calculated and averaged for each tumor.

Immunohistochemical Detection of Hypoxia

Pimonidazole hydrochloride (Hypoxyprobe-1; NPI, Belmont, MA) was injected into the tail vein at a dose of 60 mg/kg. Ninety minutes later, rats were anesthesized and then perfused for 20 minutes with physiological saline containing 5 mM $CaCl_2$. For immunohistochemistry, the tissues were immediately immersed in liquid nitrogen and stored at −80°C. After cryostat sectioning (6 μm thick), tumor sections were fixed in acetone for 5 minutes and then rehydrated in phosphate-buffered saline containing 0.1% Tween-20 (PBST) for 10 minutes. Monoclonal antibody Mab1 (NPI) that detects pimonidazole–protein adducts was diluted 1:100 and added to frozen sections followed by incubation for 2 hours at 37°C. Slides were then incubated for 1 hour at 37°C with horseradish peroxidase (HRP)–conjugated goat antimouse secondary antibody (1: 100 dilution; Serotec, Raleigh, NC). After a PBST wash, sections were immersed in AEC substrate (3-amino-9-ethylcarbazole; Vector Laboratories, Burlingame, CA) for 15 minutes at room temperature. Finally, sections were counterstained with hematoxylin and observed under light microscopy. Hypoxic fraction was determined as area positively stained for pimonidazole relative to the total tissue area using Metaview software.

Blood Vessel Density

Mouse antirat CD31 monoclonal antibody (1:20; Serotec) and HRP-conjugated goat antimouse secondary antibody (1:100) were used to detect tumor blood vessels on 6-μm sections immediately adjacent to those used for detection of hypoxia. Vascular density was evaluated using the "hot spot" technique described by Weidner [17]. The five most vascularized areas in each tumor were selected under low magnification (×4). Vascular density was determined by counting the total number of structures positive for CD31 using ×10 objective (area 0.318 mm^2) and calculating the mean number of vessels per square millimeter.

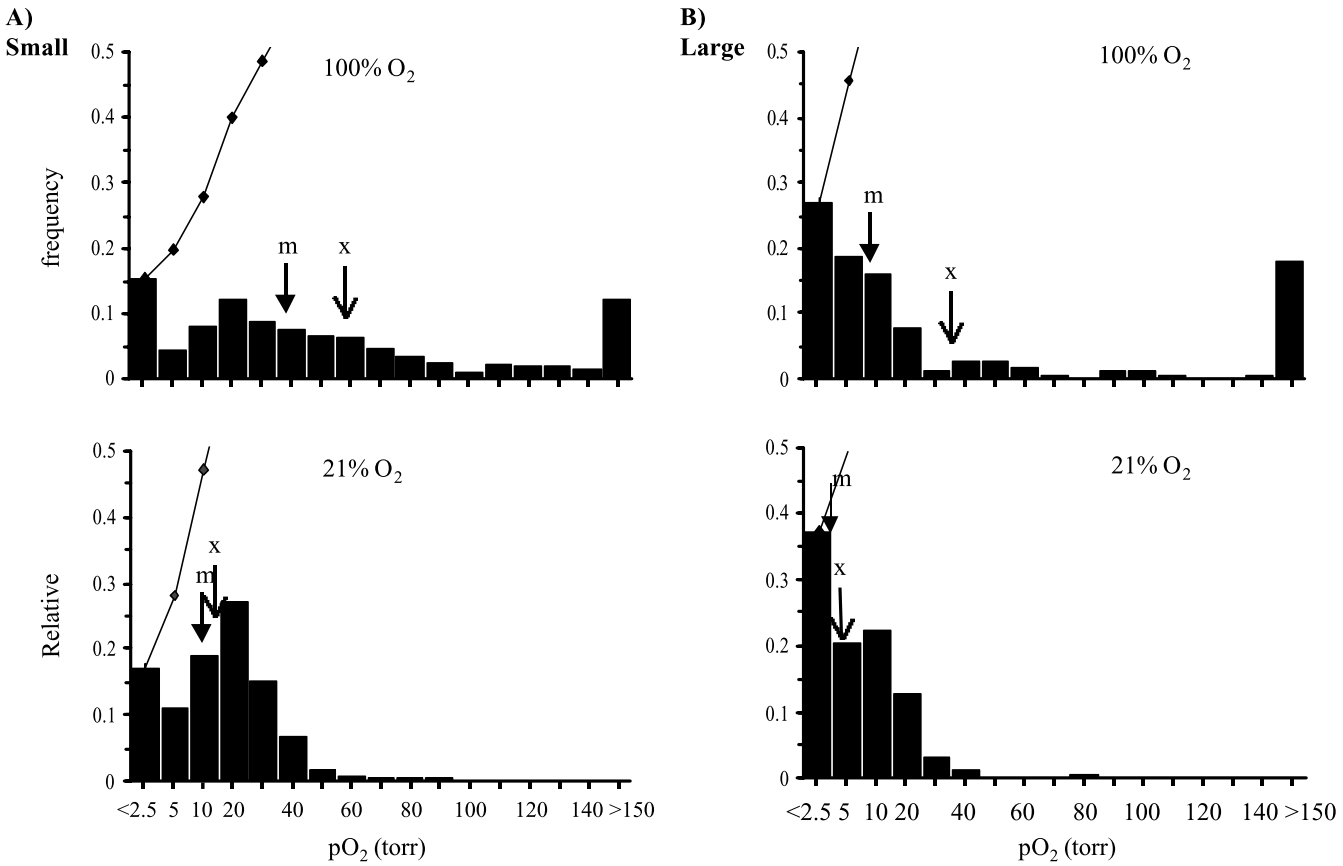

Figure 3. *Histograms of tumor oxygenation pooled for the AT1 tumors. Seven small tumors (A) (280 voxels) showed significantly higher baseline pO_2 (mean=14 ± 1 Torr, median=11 Torr) than the six large tumors (B) (149 voxels; mean = 4 ± 1 Torr, median = 3 Torr; P < 0.001). With respect to oxygen challenge, mean pO_2 in both groups increased significantly (P<.001). However, the median pO_2 in the large tumors only increased from 3 to 8 Torr. Comparison with the H tumors (Figure 2) showed that both groups of small and large AT1 tumors were less well oxygenated (P<.001). Arrows indicate mean (x) and median (m) pO_2, respectively.*

Statistical Analysis

The statistical significance of changes in oxygenation was assessed using analysis of variance (ANOVA) on the basis of Fisher's Protected Least Significant Difference (PLSD) (Statview; SAS Institute, Cary, NC). Where appropriate, the Student's *t*-test was applied. Hypoxic fractions ($HF_{2.5,5,10}$ <2.5, 5, 10 Torr) measured by *FREDOM* in all the tumors were calculated from the fraction of hypoxic voxels in each pO_2 map. All data are quoted ±SE.

Results

Tumor Oximetry — FREDOM

Overlay of ^{19}F on ^{1}H images (not shown) confirmed that HFB was widely distributed, predominantly in a central slice, and occupied voxels representing 5% to 10% of the whole tumor. In the series of EPI relaxation data sets, typically ~50 to 300 voxels provided an R1 fit and potential pO_2 value. Because even noise may give an apparent relaxation curve

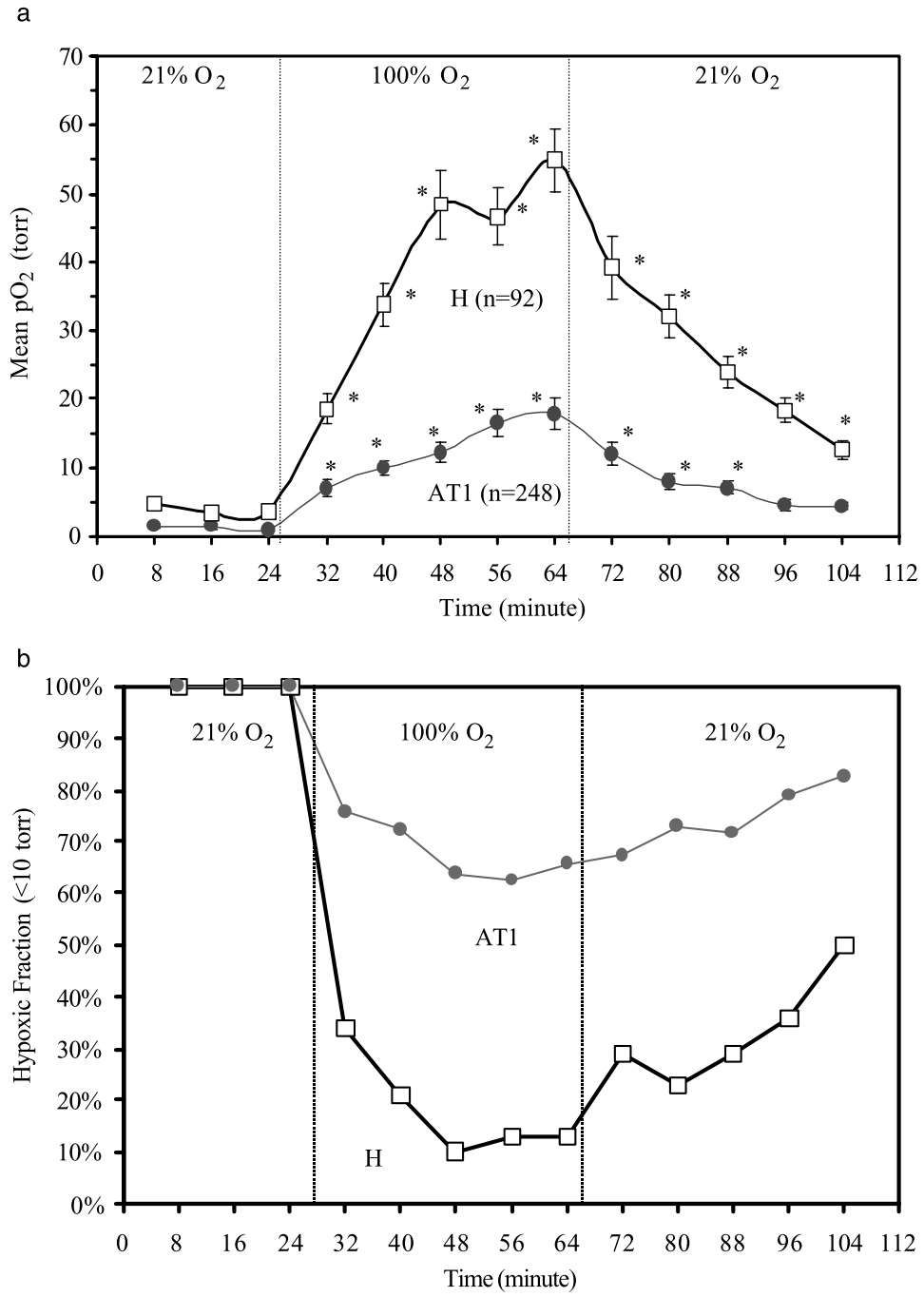

Figure 4. *Dynamic oxygenation at individual locations with initial pO_2<10 Torr (hypoxic) in response to oxygen breathing. (a) A total of 92 initially hypoxic voxels from both the small (n=31) and the large (n=61) H tumors, and 248 hypoxic voxels from the small (n=131) and large AT1 (n=117) tumors were followed with respect to gas challenge. The mean pO_2 in each subline increased immediately after oxygen breathing, and reached a mean pO_2=55±5 (SE) Torr in H versus 18±2 Torr in AT1, respectively (P<.001) after 40 minutes. (b) Dynamic hypoxic fraction (HF_{10}<10 Torr) in the initially hypoxic regions of the H tumors decreased to a minimum <10%, 24 minutes after switching to oxygen inhalation, whereas >60% initially hypoxic regions remained in the AT1 tumors (*P<.001).*

Table 1. Comparison of pO_2 Data in Individual R3327 Dunning Prostate Rat Tumors.

Tumor Subline	Size	Number	Baseline (21% O_2)				Oxygen Challenge (100% O_2)			
			pO_2 (Torr)		Hypoxic Fractions (%)		pO_2 (Torr)		Hypoxic Fractions (%)	
			Mean ± SE	Median	HF_5	HF_{10}	Mean ± SE	Median	HF_5	HF_{10}
H	Small	6	33.8 ± 4.4	30.1 ± 4.4	9 ± 2	16 ± 2	137.2 ± 22.9*	121.1 ± 21.2*	1 ± 1*	3 ± 1*
	Large	6	12.7 ± 1.1†	11.4 ± 1.6†	31 ± 4†	46 ± 5†	83.1 ± 16.2*	68.5 ± 20.0*	7 ± 3*	10 ± 4*
AT1	Small	7	10.4 ± 2.1‡	7.9 ± 2.3‡	42 ± 7‡	61 ± 7‡	62.4 ± 13.1*,‡	55.4 ± 21.0‡	19 ± 7*,‡	24 ± 9*,‡
	Large	6	3.5 ± 1.2†,‡	2.1 ± 1.0†‡	65 ± 5†,‡	83 ± 3†,‡	40.6 ± 20.1	23.2 ± 15.5	46 ± 11‡	59 ± 14‡

Small: <1.5 cm^3; large: >3 cm^3; $HF_{5\ or\ 10}$: hypoxic fraction (<5 or 10 Torr).
* *P<.05 from baseline.*
† *P<.05 from the small group.*
‡ *P<.05 from the H tumors.*

(R1) fit, data were selected within a region of interest, having T1 error <2.5 seconds and ratio T1 error/T1 <50%. With respect to respiratory interventions, only those voxels that provided consistently reliable data during the time course were included for further analysis. The number of such acceptable voxels ranged from 11 to 74 per tumor. Figure 1 shows typical pO_2 maps of the selected regions obtained from representative small H and AT1 tumors under baseline air breathing and during oxygen challenge. During air breathing, both tumors exhibited extensive heterogeneity in pO_2 distribution, but the H tumor was better oxygenated than the AT1 tumor (*P*<.001). Upon switching to oxygen breathing, both tumors responded with significantly increased mean pO_2 (*P*<.001).

Data for small and large tumors in the H and AT1 sublines are pooled as histograms in Figures 2 and 3, respectively. For the H tumors (Figure 2), a total of 219 voxels from the six small H tumors were pooled and gave a mean baseline $pO_2 = 31 \pm 2$ Torr (median = 27 Torr), which was significantly greater (*P*<.001) than for the six larger H tumors (159 voxels), which had a value of 14 ± 1 Torr (median = 12 Torr). For the AT1 subline (Figure 3), the seven small tumors (280 voxels) had a mean pO_2 of 14 ± 1 Torr (median = 11 Torr), which was significantly greater (*P*<.001) compared to the six large AT1 tumors (149 voxels; mean = 4 ± 1 Torr, median = 3 Torr). Comparison of the pooled mean baseline pO_2 between the two sublines showed that both the small and large groups of AT1 tumors had significantly lower mean pO_2 than the size-matched H groups (*P*<.001). Oxygen breathing produced significant increase in mean pO_2 in all the tumor groups (*P*<.001). However, hypoxic fractions (pO_2<2.5 Torr; 2.5<pO_2<5 Torr; 5<pO_2<10 Torr) behaved differently between the H and AT1 tumors. Specifically, for the larger tumors, the hypoxic fractions of all the ranges in the H tumors (18%, 8%, and 18%) decreased dramatically to less than 5%, whereas no distinct changes were observed in the large AT1 tumors (Figures 2 and 3).

Uniquely, *FREDOM* allows the oxygen dynamics at multiple individual locations to be followed noninvasively and simultaneously, specifically revealing the fate of initially hypoxic regions. Voxels with initial pO_2<10 Torr through all the three baseline measurements were followed with respect to respiratory challenge for both H (92 voxels) and AT1 (248 voxels) sublines (Figure 4, *a* and *b*). Figure 4*a* shows that oxygen breathing produced a significant increase in mean pO_2 for these initially hypoxic regions in both the H (mean baseline $pO_2 = 3.9 \pm 0.4$ Torr; maximum pO_2 observed with oxygen = 54.7 ± 4.6 Torr) and the AT1 (mean baseline $pO_2 = 1.2 \pm 0.1$ Torr; maximum $pO_2 = 17.9 \pm 2.3$ Torr) tumors (*P*<.01). However, comparison of the median pO_2 for these voxels showed a dramatic increase in the H tumors (baseline pO_2 = 4.1 Torr to maximum pO_2 = 46.2 Torr) *versus* only a small increase in the corresponding regions of the AT1 tumors (baseline pO_2 = 1.5 Torr to maximum pO_2 = 5.3 Torr). We also examined these hypoxic voxels grouped as having baseline pO_2<5 Torr, or in the range 5 to 10 Torr. For the AT1 tumors, both subsets behaved equivalently and in line with the trace shown in Figure 4*a*. For the H tumors, each subset showed a significant increase, but the pO_2 achieved was significantly higher for those voxels, which started in the 5- to 10-Torr group. Moreover, Figure 4*b* shows that about 90% initially hypoxic regions became well oxygenated with oxygen breathing in the H tumors, whereas >60% of the hypoxic regions in the AT1 tumors remained. Hypoxic regions in the groups of small and large AT1 tumors did not behave significantly differently (*P*>.3).

pO_2 data were also compared on the basis of differences between individual tumors, as shown in Table 1. As with the

Table 2. Comparison of Hypoxic Fraction With Histology.

Tumor Subline	*FREDOM* Hypoxic fraction (%)			Histology		
	$HF_{2.5}$	HF_5	HF_{10}	Necrosis (%)	Hypoxia Marker Pimonidazole (%)	Vascular Density CD31 (/mm^2)
H	21 ± 3	31 ± 4	46 ± 5	2 ± 1	5 ± 1	139 ± 30
AT1	51 ± 5*	65 ± 5*	83 ± 3*	7 ± 1	18 ± 4*	45 ± 13*

$HF_{2.5,\ 5\ or\ 10}$: hypoxic fraction (<2.5, 5, or 10 Torr).
**P<.05 from H tumors.*

pooled data, for both the H and AT1 tumors, the large tumors were significantly more hypoxic than the smaller tumors, and the AT1 tumors were significantly less well oxygenated than the size-matched H tumors ($P<.05$; Tables 1 and 2). With respect to oxygen challenge, all the tumors in the H subline and the small AT1 showed significant increases in global mean pO_2 ($P<.001$), whereas three of six larger AT1 tumors did not respond to oxygen. The mean and median pO_2 increased, and the $HF_{5\ or\ 10}$ decreased significantly in the H and the small AT1 tumors with oxygen inhalation ($P<.05$; Table 1). Mean pO_2 of the group of six large tumors did increase, but only reached a $P<.1$ level of significance.

Immunohistochemistry

AT1 tumors were significantly more hypoxic than the H tumors of comparable size (Figure 5 and Table 2). The positive staining for pimonidazole in the AT1 tumors was primarily detected in tumor cells located in perinecrotic regions and more than 100 μm away from blood vessels, which were recognized by the anti-CD31 antibody (Figure 5, *C* and *D*). The total number of vessels per square millimeter was 139 ± 30 (range 88–227) in the better-oxygenated H tumors, which was significantly higher than for the more hypoxic AT1 tumors ($45 \pm 13/mm^2$, range 28–71, $P<.05$; Figure 5 and Table 2). This difference in vascularity also coincided with the greater necrotic fraction: about 7% area in the AT1 tumors compared with only 2% in the H tumors (Table 2).

Discussion

The anaplastic and faster-growing AT1 tumors were significantly more hypoxic than the well-differentiated and slower-growing H tumors from which they were originally derived. These results are consistent with previous reports comparing oxygenation and radiation sensitivity of the AT and H sublines. Based on electrode polarographic pO_2 measurements, the H subline was found to be considerably less hypoxic [18]. This coincided with [^{31}P]NMR showing

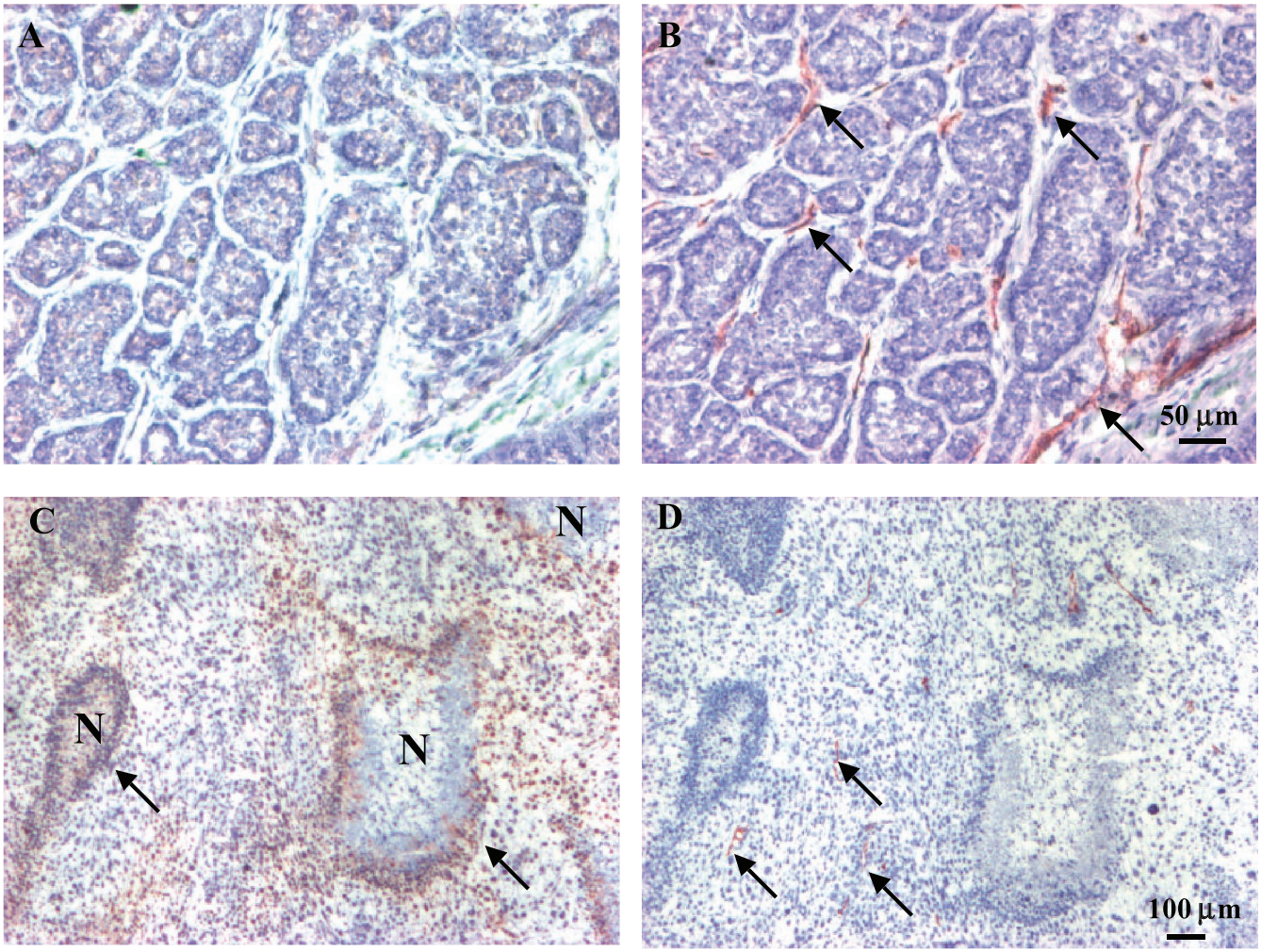

Figure 5. *Distribution of pimonidazole and CD31 in representative large H and AT1 tumors (A) Well-differentiated H tumor comprising multiple glandular structures and connective stroma. Immunostaining for hypoxia marker, pimonidazole showed few positive cells. (B) Anti-CD31 staining (brown) demonstrated relatively well-distributed vascular endothelial cells in a consecutive 6-μm section. (C) The anaplastic AT1 tumor is composed of nonglandular structure and fewer stromal cells. Typical distribution of hypoxia in the AT1, recognized as positive staining for pimonidazole (brown), was observed at some distance from blood vessels stained for CD31 (D, arrow) and located adjacent to necrotic regions (N).*

greater phosphocreatine and less inorganic phosphate (Pi) in H tumors [19]. Moreover, radiation sensitivity of AT, but not H, tumors could be enhanced by misonidazole [20], suggesting a lack of hypoxia in the H tumors. We have ourselves examined AT1 tumors previously during the development of the [^{19}F]MRI oximetry technique [8,21]. The mean and median pO_2 values reported now and previously are remarkably similar, together with distribution histograms and hypoxic fractions. In all cases, we have found that larger tumors are significantly less well oxygenated than small tumors and, indeed, this was also observed in other Dunning prostate R3327 tumors sublines (MAT-Lu and HI) [9,22] and rat breast tumors [23]. Yeh et al. [18] found no such correlation with size for either subline based on electrode oximetry, but ^{31}PNMR did show metabolic hypoxiation in larger AT tumors [19]. Interlaboratory comparison must recognize differences in techniques and procedures. The histology of our tumors is very similar to that of Yeh et al. [18] and Thorndyke et al. [20], and growth of the H tumors is comparable. However, we work with the AT1 subline [10], as opposed to the AT, and we find a VDT of 5 days as opposed to 2 or 3 days [20]. In comparing our own previous data, we have now altered our anesthesia protocol to a baseline of air/isoflurane as opposed to 33% oxygen in nitrous oxide with metafane [8,21]. Nonetheless, the pO_2 distributions appear very similar.

In addition to providing tumor baseline pO_2, the *FREDOM* technique allows the study of oxygen dynamics in response to interventions (e.g., respiratory challenge). Our results show that oxygen breathing produced significant increase in mean pO_2 in all the H tumors and the small AT1 tumors, whereas the change was only borderline significant in the larger AT1 tumors (Table 1). Most interestingly, the initially hypoxic regions in the H tumors responded significantly to become well oxygenated with oxygen challenge, whereas no distinct reduction in hypoxic fractions was observed in the large AT1 tumors (Table 1 and Figure 4, *a* and *b*). The AT1 tumor data coincide with our previous observations in this subline [21].

There is increasing evidence that tumor malignant progression may be associated with a hypoxic microenvironment [5,6,24]. Several recent clinical studies have demonstrated a positive relationship between the presence of hypoxia and poor outcome associated with malignant progression and metastasis in several cancers (e.g., advanced squamous cell carcinoma of the cervix [3,25,26], and sarcomas and carcinomas from head, neck, and soft tissue [27]). Studies of breast cancer have not all been consistent. For example, early work by Vaupel et al. [28] showed no correlation between grade or stage and pO_2 using the Eppendorf Histograph. By contrast, a recent report from Hohenberger et al. [29] indicated that mean pO_2 and hypoxic fraction in breast tumors were associated with both grade and stage. The results of Höckel et al. [3] in advanced cervical cancer patients showed a lack of correlation between tumor oxygenation and differentiation or stage, but a significantly positive correlation of tumor oxygenation and malignant progression. In an animal model, Thews et al. [30] reported that a higher differentiated rhabdomyosarcoma subline, F1, of the BA-HAN-1 was less well oxygenated than the undifferentiated G8 subline. Although the results of Thews et al. show the opposite trend to the observations we report here, it is important to note that the F1 and G8 tumors grow relatively rapidly. In our studies, the higher differentiated tumors grow much more slowly. Several other studies have shown evidence that tumor malignant progression (e.g., local invasion, destructive growth and metastasis) may be associated with hypoxic microenvironment in both experimental models [5,24,31,32] and the clinic [25,26,33]. A recent study by Movsas et al. [34] using the Eppendorf Histograph showed that increasing levels of hypoxia were related to increasing clinical stage of human prostate carcinomas, but trends with respect to grade did not reach significance. Eble et al. [35] found that the moderately well-differentiated Dunning rat prostate HI subline was better oxygenated than the anaplastic AT1 subline, and Yeh et al. [18] found that the well-differentiated H subline was better oxygenated than the anaplastic AT. Our previous study of two other Dunning prostate R3327 rat tumor sublines showed that the poorly differentiated and faster-growing (VDT=2.7 days) and metastatic MAT-Lu tumors were less well oxygenated than the moderately differentiated and slower-growing (VDT=9 days) HI tumors. Similar to the results here, breathing hyperoxic gas (oxygen or carbogen) significantly increased the oxygenation and reduced the hypoxic fraction in the HI tumors, but to a much lesser extent in the metastatic MAT-Lu tumors [9]. This would tend to support the hypothesis that tumor hypoxia is associated with parameters such as increased growth rate and level of differentiation (grade). As in our previous studies [9,22,23] of various tumor types, tumor size, which is a major component of tumor staging, showed a strongly inverse relationship to oxygenation.

Many experimental and clinical studies have demonstrated that reoxygenation of hypoxic tumor cells contributes to improved radiation sensitivity for tumor therapy [36,37]. Whether initially hypoxic regions of a tumor can be modified to become better oxygenated has long been considered a key indicator for outcome of irradiation. Examining the initially hypoxic regions (pO_2<10 Torr) showed that more than 90% of the hypoxic regions in the H tumors became better oxygenated in response to oxygen breathing. In contrast, about 60% of such regions from the AT1 tumors remained unchanged (Figure 4*b*). Thus, one would expect that radiosensitivity of the H tumors might be significantly improved with pretreatment oxygen breathing, whereas beneficial effect in the AT1 tumors would be less. In fact, measurements in HI tumors with respect to our recent experimental radiotherapy have validated the hypothesis. We found that oxygen breathing before and during a 30-Gy single-dose irradiation significantly enhanced the radiosensitivity by prolonging the tumor growth delay in large HI tumors [38]. Intriguingly, breathing oxygen had no benefit in small HI tumors coinciding with a very small baseline hypoxic fraction. By analogy, one would expect that patients with hypoxic tumors like the large H and HI would show

enhanced local control by irradiation in combination with oxygen breathing. Actually, recent clinical data have shown promising results in advanced head and neck cancers accomplished by accelerated radiotherapy with the carbogen and nicotinamide (ARCON) schedule. The phase II trial demonstrated that the ARCON has significantly improved 3-year local control rates to 80% for larynx, 69% for hypopharynx, 88% for oropharynx cancers [39], and those patients with hypoxic tumors received the greatest benefit from the ARCON paradigm [33].

Comparison of Figure 4, *a* and *b* shows that the mean pO_2 in the initially hypoxic regions from both the H and the AT1 tumors continued to increase during the course of 40-minute oxygen breathing, whereas the corresponding hypoxic fraction in both sublines dropped to a minimum value within 24 minutes and then remained stable. This discrepancy suggests that hypoxic regions may be divided into two categories: those that are modulated by oxygen within 24 minutes and continue to show increase at later times, *versus* those that are unresponsive. This information could be valuable for guiding and planning radiotherapy. In our previous studies of the Dunning prostate rat tumors, we found that oxygen or carbogen breathing produced a similar effect on tumor oxygenation across all the sublines MAT-Lu, AT1, and HI [8,9,21,22,40]. Our irradiation study validated that oxygen breathing significantly improved radiosensitivity in initially hypoxic large HI tumors [38].

HFB has many strengths as a reporter molecule: MR interrogation is nondestructive, and HFB exhibits remarkably low toxicity and is readily available. From an MR perspective, HFB is ideal, having a single resonance, high sensitivity to pO_2, and minimal sensitivity to temperature [41]. The high vapor pressure produces a short biological half-life ($T_{1/2} \sim 600$ minutes) [40], but there is little macroscopic redistribution over a period of 2.5 hours allowing effective investigations of acute interventions [41]. The Hamilton syringe with a custom-made fine sharp needle (32 gauge) was designed to minimize tissue damage. Our current data, as well as our previous observations, have demonstrated the stability of local pO_2 measurements under baseline conditions. *FREDOM* oximetry has been validated by various techniques in previous studies (e.g., similar baseline pO_2 distribution in the AT1 tumors acquired by Eppendorf Histograph [21] and comparable oxygen dynamics with oxygen or carbogen challenge observed in HI tumors using the fiber optic OxyLite [22] or oxygen electrodes [9]).

Tumor oxygenation may be investigated at many levels, ranging from induced gene expression to cellular microscopy and macroscopic techniques. Ultimately, correlation with outcome is relevant to clinical application, as has been demonstrated for measurements using the Eppendorf Histograph [3,26,27] and, most recently, pimonidazole binding [33]. We have previously shown that pO_2 measurements using *FREDOM* were similar to the Histograph and now we show that hypoxic fractions are commensurate with pimonidazole binding. The anaplastic and faster-growing AT1 tumors had significantly higher pimonidazole binding (18%) than the well-differentiated and slower-growing H tumors (5%, $P<.05$), consistent with the *FREDOM* measurements. However, as shown in Table 2, the hypoxic fractions $HF_{2.5,5,10}$ measured by *FREDOM* for the large AT1 tumors were far greater than the extent of pimonidazole binding. Others have also reported such discrepancies using Histograph or OxyLite [12,42]. Histograph assessment of oxygenation does not differentiate hypoxic live tissues from necrotic regions, leading to overestimation of tumor hypoxia [43,44]. However, in our tumors, the level of necrosis is relatively small and would not account for the disparity. It has also been suggested that diffusion may limit the distribution of bioreductive hypoxia markers, leading to underestimation of tumor hypoxia [45] and, in addition, nitroimidazole binding may be influenced by levels of both nitroreductase and thiol [46]. Furthermore, a pO_2 threshold value for hypoxic marker binding is not clearly defined *in vivo*. There may also be differences in sensitivity to chronic *versus* acute hypoxia and the time required for efficient pimonidazole labeling. Bennewith et al. [47] have now shown significantly greater pimonidazole binding when assessed following 96 hours of continuous oral availability, as opposed to a single intravenous or intraperitoneal dose followed by tissue harvest after 6 hours. Here, we followed the manufacturer's recommendations of a 90-minute delay between intravenous administration and sacrifice. Despite the lack of absolute correspondence, a general positive correlation in assessments of tumor hypoxia has been reported between Histograph or OxyLite and pimonidazole binding by others [12,44], and now by us here.

Tumor hypoxia results, in part, from inadequate blood vessel development and solid tumors appear not to grow beyond a critical size of ~ 1 mm^3 without evoking angiogenesis [48]. Figure 5 shows a typical case of insufficient blood vessels in a region of an AT1 tumor, which results in hypoxia and eventually necrosis with increased distance away from the vessels. The anti-CD31 staining for vascular endothelial cells showed that the more hypoxic AT1 tumors had lower vascular density than the better-oxygenated H tumors (Table 2). This result is in agreement with other reports in various animal or human tumors indicating greater hypoxia at reduced vascular density [11,44]. However, some studies have shown the opposite trend [17,49], may be because hypoxia stimulates angiogenesis, generating greater neovasculature. Here, we have applied histological approaches to assess hypoxia in relation to vascular density. Others have examined additional pertinent parameters including vascular perfusion (e.g., using distribution of the Hoechst 33342 dye) [14,38] and even dynamic changes by applying pairs of distinct hypoxia markers (CCI-103F and pimonidazole) sequentially before and after an intervention to reveal dynamic response (pulse chase double labeling) [14]. Specifically, they were able to detect changes in tumor hypoxia following interventions designed to modulate hypoxia such as breathing hyperoxic gas and hydralazine. Ultimately, dynamic studies will be of great importance, and the availability and correlation of many diverse techniques revealing tissue and cellular properties on various scales from whole tumor to microscopic resolution will be pertinent.

The *FREDOM* approach to tumor oximetry has the great advantage of facilitating noninvasive assessment of changes in pO_2 in response to interventions, as shown here for breathing hyperoxic gases and previously for vasoactive agents, such as hydralazine [50], or vascular targeting agents [51]. The method is inherently quantitative, but it does require introduction of small quantities (~ 50 μl) of the reporter molecule, HFB. Another drawback for potential clinical application is the current lack of an [^{19}F]NMR channel on most clinical MRI scanners. Currently, we estimate that at least 20 research instruments in the world have a clinical [^{19}F]EPI capability and this will increase dramatically with the popularity of high field systems (e.g., 3 T). Our own institution is installing its first clinical [^{19}F]MRI capability in spring 2003 and we envisage clinical application of the *FREDOM* in the near future. We are currently investigating Investigational New Drug approval for HFB.

We and others are also searching for alternative noninvasive approaches. Near-infrared reveals changes in vascular oxygenation with high time resolution, but currently little spatial discrimination [52]. BOLD (Blood Oxygen Level–Dependent) contrast [^{1}H]MRI provides spatial resolution and is sensitive to changes in vascular oxygenation, but also is sensitive to changes in tumor blood flow and tumor blood volume (FLOOD) [53]. Moreover, correlations between changes in signal intensity and direct measures of pO_2 have shown a qualitative relationship, but poor indication of absolute pO_2 [54,55]. In some cases, correlation has been shown between pO_2 and dynamic contrast-enhanced (DCE) [^{1}H]MRI [56,57], but although DCE can reveal changes in vascular flow and permeability, it must be recognized that tissue pO_2 represents a balance between oxygen delivery and consumption, and thus, such correlations are unlikely to be valid across diverse tumor types.

In conclusion, we have demonstrated that in comparison with the H tumor, the anaplastic and faster-growing AT1 subline of the Dunning R3327 tumor is significantly more hypoxic. Comparable data using histological markers of hypoxia and vascular endothelium further validate the assessment of tumor oxygenation by *FREDOM*. We believe this approach can provide valuable insight into tumor physiology and response to interventions, assisting in the development of novel therapeutic strategies. Ultimately, *FREDOM* should have application in the clinical setting.

Acknowledgements

We are grateful to Matthew Merritt for maintaining the MR system, Maria Sambade for assistance with histology, Peter Peschke (DKFZ) for providing tumor cells, and Philip Thorpe for laboratory facilities.

References

[1] Brown JM, and Giaccia AJ (1994). Tumor hypoxia: the picture has changed in the 1990s. *Int J Radiat Biol* **65,** 95–102.

[2] Denekamp J (1989). Physiological hypoxia and its influence on radiotherapy. In *The Biological Basis of Radiotherapy*, 2nd ed. GG Steel, GE Adams, and A Horwich, Eds. Elsevier, Amsterdam. pp. 115–43.

[3] Höckel M, Schlenger K, Aral B, Mitze M, Schäffer U, and Vaupel P (1996). Association between tumor hypoxia and malignant progression in advanced cancer of the uterine cervix. *Cancer Res* **56,** 4509–515.

[4] Sartorelli AC (1988). Therapeutic attack of hypoxic cells of solid tumors: presidential address. *Cancer Res* **48,** 775–78.

[5] De Jaeger K, Kavanagh MC, and Hill RP (2001). Relationship of hypoxia to metastatic ability in rodent tumors. *Br J Cancer* **84,** 1280–285.

[6] Höckel M, and Vaupel P (2001). Tumor hypoxia: definitions and current clinical, biologic, and molecular aspects. *J Natl Cancer Inst* **93,** 266–76.

[7] Stone HB, Brown JM, Phillips T, and Sutherland RM (1993). Oxygen in human tumors: correlations between methods of measurement and response to therapy. *Radiat Res* **136,** 422–34.

[8] Hunjan S, Zhao D, Constantinescu A, Hahn EW, Antich PP, and Mason RP (2001). Tumor oximetry: demonstration of an enhanced dynamic mapping procedure using fluorine-19 echo planar magnetic resonance imaging in the Dunning prostate R3327-AT1 rat tumor. *Int J Radiat Oncol Biol Phys* **49,** 1097–108.

[9] Zhao D, Constantinescu A, Hahn EW, and Mason RP (2002). Differential oxygen dynamics in two diverse Dunning prostate R3327 rat tumor sublines (MAT-Lu and HI) with respect to growth and respiratory challenge. *Int J Radiat Oncol Biol Phys* **53,** 744–56.

[10] Isaacs J, Isaacs W, Feitz W, and Scheres J (1986). Establishment and characterization of 7 Dunning prostate cancer cell lines and their use in developing methods for predicting metastatic ability of prostate cancer. *Prostate* **9,** 261–81.

[11] Vaupel P, Kallinowski F, and Okunieff P (1989). Blood flow, oxygen and nutrient supply, and metabolic microenvironment of human tumors: a review. *Cancer Res* **49,** 6449–465.

[12] Raleigh JA, Chou SC, Arteel GE, and Horsman MR (1999). Comparison among pimonidazole binding, oxygen electrode measurements, and radiation response in C3H mouse tumors. *Radiat Res* **151,** 580–89.

[13] Evans SM, Hahn S, Pook DR, Jenkins WT, Chalian AA, Zhang P, Stevens C, Weber R, Weinstein G, Benjamin I, Mirza N, Morgan M, Rubin S, McKenna WG, Lord EM, and Koch CJ (2000). Detection of hypoxia in human squamous cell carcinoma by EF5 binding. *Cancer Res* **60,** 2018–2024.

[14] Ljungkvist ASE, Bussink J, Rijken PFJW, Raleigh JA, Denekamp J, and Van Der Kogel AJ (2000). Changes in tumor hypoxia measured with a double hypoxic marker technique. *Int J Radiat Oncol Biol Phys* **48,** 1529–538.

[15] Peschke P, Hahn EW, Wenz F, Lohr F, Braunschweig F, Wolber G, Zuna I, and Wannenmacher M (1998). Differential sensitivity of three sublines of the rat Dunning prostate tumor system R3327 to radiation and/or local tumor hyperthermia. *Radiat Res* **150,** 423–30.

[16] Hahn EW, Peschke P, Mason RP, Babcock EE, and Antich PP (1993). Isolated tumor growth in a surgically formed skin pedicle in the rat: a new tumor model for NMR studies. *Magn Reson Imaging* **11,** 1007–1017.

[17] Weidner N (1995). Intratumor microvessel density as a prognostic factor in cancer. *Am J Pathol* **147,** 9–19.

[18] Yeh KA, Biade S, Lanciano RM, Brown DQ, Fenning MC, Babb JS, Hanks GE, and Chapman JD (1995). Polarographic needle electrode measurements of oxygen in rat prostate carcinomas: accuracy and reproducibility. *Int J Radiat Oncol Biol Phys* **33,** 111–18.

[19] Chapman JD, McPhee MS, Walz N, Chetner MP, Stobbe CC, Soderlind K, Arnfield M, Meeker BE, Trimble L, and Allen PS (1991). Nuclear magnetic resonance spectroscopy and sensitizer-adduct measurements of photodynamic therapy–induced ischemia in solid tumors. *J Natl Cancer Inst* **83,** 1650–659.

[20] Thorndyke C, Meeker B, Thomas G, Laky W, McPhee M, and Chapman J (1985). The radiation sensitivities of R3327-H and -AT1 rat prostate adenocarcinomas. *J Urol* **134,** 191–98.

[21] Mason RP, Constantinescu A, Hunjan S, Le D, Hahn EW, Antich PP, Blum C, and Peschke P (1999). Regional tumor oxygenation and measurement of dynamic changes. *Radiat Res* **152,** 239–49.

[22] Zhao D, Constantinescu A, Hahn EW, and Mason RP (2001). Tumor oxygen dynamics with respect to growth and respiratory challenge: investigation of the Dunning prostate R3327-HI tumor. *Radiat Res* **156,** 510–20.

[23] Song Y, Constantinescu A, and Mason RP (2002). Dynamic breast tumor oximetry: the development of prognostic radiology. *Technol Cancer Res Treat* **1,** 1–8.

[24] Rofstad EK (2000). Microenvironment-induced cancer metastasis. *Int J Radiat* **76,** 589–605.

[25] Birner P, Schindl P, Obermair A, Plank C, Breitenecker G, and Oberhuber G (2000). Overexpression of hypoxia-inducible factor 1 is a

marker for an unfavorable prognosis in early-stage invasive cervical cancer. *Cancer Res* **60,** 4693–696.
[26] Fyles A, Milosevic M, Hedley M, Pintile M, Levin W, Manchul L, and Hill RP (2002). Tumor hypoxia has independent predictor impact only on patients with node-negative cervix cancer. *J Clin Oncol* **20,** 680–87.
[27] Brizel DM, Scully SP, Harrelson JM, Layfield LJ, Bean JM, Prosnitz LR, and Dewhirst MW (1996). Tumor oxygenation predicts for the likelihood of distant metastases in human soft tissue sarcoma. *Cancer Res* **56,** 941–43.
[28] Vaupel PW, Schlenger K, Knoop C, and Höckel M (1991). Oxygenation of human tumors: evaluation of tissue oxygen distribution in breast cancers by computerized O_2 tension measurements. *Cancer Res* **51,** 3316–322.
[29] Hohenberger P, Felger C, Haensch W, and Schlag PM (1998). Tumor oxygenation correlates with molecular growth determinants in breast cancer. *Breast Cancer Res Treat* **48,** 97–106.
[30] Thews O, Kelleher DK, Lecher B, and Vaupel P (1998). Blood flow, oxygenation, metabolic and energetic status in different clonal subpopulations of a rat rhabdomyosarcoma. *Int J Oncol* **13,** 205–11.
[31] Young S, Marshall R, and Hill R (1988). Hypoxia induces DNA overreplication and enhances metastatic potential of murine tumor cells. *Proc Natl Acad Sci USA* **85,** 9533–537.
[32] Cairns RA, Kalliomaki T, and Hill RP (2001). Acute (cyclic) hypoxia enhances spontaneous metastasis of KHT murine tumors. *Cancer Res* **61,** 8903–908.
[33] Kaanders JHAM, Wijffels KIEM, Marres HAM, Ljungkvist ASE, Pop LAM, van den Hoogen FJA, de Wilde PCM, Bussink J, Raleigh JA, and van der Kogel AJ (2002). Pimonidazole binding and tumor vascularity predict for treatment outcome in head and neck cancer. *Cancer Res* **62,** 7066–7074.
[34] Movsas B, Chapman J, Greenberg R, Hanlon A, Horwitz E, Pinover W, Stobbe C, and Hanks G (2000). Increasing levels of hypoxia in prostate carcinoma correlate significantly with increasing clinical stage and patient age: an Eppendorf pO_2 study. *Cancer* **89,** 2018–2024.
[35] Eble MJ, Lohr F, Wenz F, Krems B, Bachert P, and Peschke P (1995). Tissue oxygen tension distribution in two sublines of the Dunning prostate tumor R3327. In *Tumor Oxygenation.* PW Vaupel, DK Kelleher, and M, Gunderoth, Eds. Funktionsanalyse Biologischer Systeme, Gustav Fischer Verlag, Stuttgart. pp. 95–105.
[36] Kallman R, and Dorie M (1986). Tumor oxygenation and reoxygenation during radiation therapy: importance in predicting tumor response. *Int J Radiat Oncol Biol Phys* **12,** 681–85.
[37] Fenton BM (1997). Effects of carbogen plus fractionated irradiation on KHT tumor oxygenation. *Radiother Oncol* **44,** 183–90.
[38] Zhao D, Constantinescu A, Chang CK, Hahn EW, and Mason RP (2003). Correlation of tumor oxygen dynamics with radiation response of the Dunning prostate R3327-HI tumors. *Radiat Res* **159,** 621–31.
[39] Kaanders JHAM, Pop LAM, Marres HAM, Bruaset I, van den Hoogen FJA, Merkx MAW, and van der Kogel AJ (2002). ARCON: experience in 215 patients with advanced head-and-neck cancer. *Int J Radiat Oncol Biol Phys* **52,** 769–78.
[40] Hunjan S, Mason RP, Constantinescu A, Peschke P, Hahn EW, and Antich PP (1998). Regional tumor oximetry: ^{19}F NMR spectroscopy of hexafluorobenzene. *Int J Radiat Oncol Biol Phys* **40,** 161–71.
[41] Mason RP, Rodbumrung W, and Antich PP (1996). Hexafluorobenzene: a sensitive ^{19}F NMR indicator of tumor oxygenation. *NMR Biomed* **9,** 125–34.
[42] Bussink J, Kaanders JHAM, Strik AM, Vojnovic B, and van der Kogel AJ (2000). Optical sensor-based oxygen tension measurements correspond with hypoxia marker binding in three human tumor xenograft lines. *Radiat Res* **154,** 547–55.
[43] Evans SM, Hahn S, Hahn SM, Magarelli DP, and Koch CJ (2001). Hypoxic heterogeneity in human tumors: EF5 binding, vasculature, necrosis, and proliferation. *Am J Clin Oncol* **24,** 467–72.
[44] Lyng H, Sundfor K, and Rofstad EK (1997). Oxygen tension in human tumours measured with polarographic needle electrodes and its relationship to vascular density, necrosis and hypoxia. *Radiother Oncol* **44,** 163–69.
[45] Olive PL (1994). Radiation-induced reoxygenation in the SCC VII murine tumor: evidence for a decrease in oxygen consumption and an increase in tumor perfusion. *Radiother Oncol* **32,** 37–46.
[46] Jenkins WT, Evans SM, and Koch CJ (2000). Hypoxia and necrosis in rat 9L glioma and Morris 7777 hepatoma tumors: comparative measurements using EF5 binding and the Eppendorf needle electrode. *Int J Radiat Oncol Biol Phys* **46,** 1005–1017.
[47] Bennewith KL, Raleigh JA, and Durand RE (2002). Orally administered pimonidazole to label hypoxic tumor cells. *Cancer Res* **62,** 6827–830.
[48] Folkman J (1974). Tumor angiogenesis. *Adv Cancer Res* **19,** 331–58.
[49] Semenza GL (2002). HIF-1 and tumor progression: pathophysiology and therapeutics. *Trends Mol Med* **8,** S62–67.
[50] Zhao D, Constantinescu A, Jiang L, Hahn EW, and Mason RP (2001). Prognostic radiology: quantitative assessment of tumor oxygen dynamics by MRI. *Am J Clin Oncol* **24,** 462–66.
[51] Mason RP, Ran S, and Thorpe PE (2002). Quantitative assessment of tumor oxygen dynamics: molecular imaging for prognostic radiology. *J Cell Biochem* **87,** 45–53.
[52] Kim JG, Zhao D, Song Y, Constantinescu A, Mason RP, and Liu H (2003). Interplay of tumor vascular oxygenation and tumor pO_2 observed using NIRS, oxygen electrode, and ^{19}F MR pO_2 mapping. *J Biomed Opt* **8,** 53–62.
[53] Howe FA, Robinson SP, Rodrigues LM, and Griffiths JR (1999). Flow and oxygenation dependent (FLOOD) contrast MR imaging to monitor the response of rat tumors to carbogen breathing. *Magn Reson Imaging* **17,** 1307–318.
[54] Baudelet C, and Gallez B (2002). How does blood oxygen level-dependent (BOLD) contrast correlate with oxygen partial pressure (pO_2) inside tumors? *Magn Reson Med* **48,** 980–86.
[55] Fan X, River JN, Zamora M, Al-Hallaq HA, and Karczmar GS (2002). Effect of carbogen on tumor oxygenation: combined fluorine-19 and proton MRI measurements. *Int J Radiat Oncol Biol Phys* **54,** 1202–209.
[56] Cooper RA, Carrington BM, Loncaster JA, Todd SM, Davidson SE, Logue JP, Luthra AD, Jones AP, Stratford I, Hunter RD, and West CML (2000). Tumor oxygenation levels correlate with dynamic contrast-enhanced magnetic resonance imaging parameters in carcinoma of the cervix. *Radiother Oncol* **57,** 53–59.
[57] Wang Z, Su M-Y, and Nalcioglu O (2002). Applications of dynamic contrast enhanced MRI in oncology: measurement of tumor oxygen tension. *Technol Cancer Res Treat* **1,** 29–38.